Adhesion and Wetting of Soft Nanoparticles on Textured Surfaces: Transition between Wenzel and Cassie–Baxter States

ARTICLE *in* LANGMUIR · JANUARY 2015

Impact Factor: 4.46 · DOI: 10.1021/la5045442 · Source: PubMed

4 AUTHORS, INCLUDING:

Jan-Michael Carrillo

Oak Ridge National Laboratory

63 PUBLICATIONS **578** CITATIONS

SEE PROFILE

Andrey V Dobrynin

University of Akron

124 PUBLICATIONS **4,912** CITATIONS

SEE PROFILE

Langmuir

Article

pubs.acs.org/Langmuir

Adhesion and Wetting of Soft Nanoparticles on Textured Surfaces: Transition between Wenzel and Cassie–Baxter States

Zhen Cao,[†] Mark J. Stevens,[‡] Jan-Michael Y. Carrillo,[§] and Andrey V. Dobrynin*[,†]

[†]Polymer Program and Institute of Materials Science, University of Connecticut, Storrs, Connecticut 06269-3136, United States
[‡]Center for Integrated Nanotechnologies, Sandia National Laboratories, Albuquerque, New Mexico 87185-1315, United States
[§]National Center for Computational Science, Oak Ridge National Laboratory, Oak Ridge, Tennessee 37831, United States

ABSTRACT: We use a combination of the molecular dynamics simulations and scaling analysis to study interactions between gel-like nanoparticles and substrates covered with rectangular shape posts. Our simulations have shown that nanoparticles in contact with substrate undergo a first-order transition between the Cassie–Baxter and Wenzel states, which depends on nanoparticle shear modulus, the strength of nanoparticle–substrate interactions, height of the substrate posts, and nanoparticle size, R_p. There is a range of system parameters where these two states coexist such that the average indentation δ produced by substrate posts changes with nanoparticle shear modulus, G_p. We have developed a scaling model that describes deformation of nanoparticle in contact with patterned substrate. In the framework of this model, the effect of the patterned substrate can be taken into account by introducing an effective work of adhesion, W_{eff}, which describes the first-order transition between Wenzel and Cassie–Baxter states. There are two different shape deformation regimes for nanoparticles with shear modulus G_p and surface tension γ_p. The shape of small nanoparticles with size $R_p < \gamma_p^{3/2}G_p^{-1}W_{eff}^{-1/2}$ is controlled by capillary forces, while deformation of large nanoparticles, $R_p > \gamma_p^{3/2}G_p^{-1}W_{eff}^{-1/2}$, is determined by nanoparticle elastic and contact free energies. The model predictions are in good agreement with simulation results.

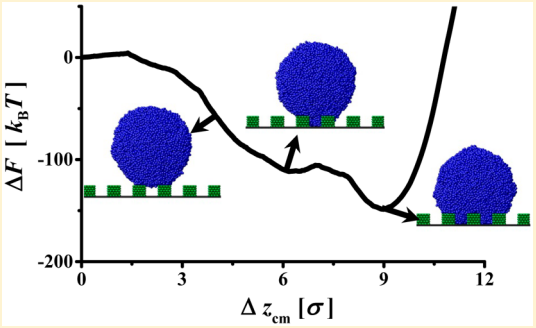

1. INTRODUCTION

Design of functional and responsive surfaces with well-controlled wettability and adhesion characteristics has emerged as one of the fast developing areas of materials science.[1−3] Biological surfaces with unique wetting and adhesion characteristics inspired design principles for creating artificial surfaces mimicking the self-cleaning ability of lotus leaves[4,5] and fish scales,[6] antifogging functionality of mosquito eyes,[7] high adhesion of gecko feet,[6,8] and water collection properties of spider silk and cactus.[9,10] These remarkable properties of biological surface arise from their multiscale textured structure (see, for review, ref 2).

Interactions of liquids and elastic solids with textured or rough surfaces are different from interactions with smooth substrates.[1,3,11] Changes in the surface roughness or texture pattern produce variations in the effective contact area. For example, the values of the contact angle of liquid droplets measured on structured (rough) surfaces are different from those observed on smooth surfaces (see Figure 1). A droplet in contact with a textured surface to minimize system free energy can adopt one of three configurations, the Wenzel,[12] the Cassie–Baxter,[13,14] or the Cassie impregnating state.[15,16] In the Wenzel state (Figure 1b), the liquid conforms to all topographical features of the textured (rough) surface, producing a fully wetted surface. In this case, the value of the apparent contact angle θ^* on the surface with the roughness parameter $r \geq 1$ accounting for the increase of the effective contact area between a droplet and a surface is given by the Wenzel expression:

$$\cos\theta^* = r\cos\theta \tag{1}$$

Because the surface roughness parameter $r \geq 1$, the surface roughness always magnifies the wetting properties of the substrate. In the Cassie–Baxter state (see Figure 1c), the trapped air prevents liquid from completely wetting a surface. Therefore, the surface can be viewed as a heterogeneous surface characterized by two contact angles 180° and θ corresponding to contact between solid–liquid–air. The apparent contact angle in this state is calculated by using the Cassie–Baxter expression:

$$\cos\theta^* = -(1 - f_S) + f_S\cos\theta \tag{2a}$$

where f_s is the fraction of the surface in contact with liquid under the drop. It follows from eq 2a that the surface texture could increase substrate hydrophobicity through the air trapping mechanism. In a particular range of the surface roughness and hydrophobicity, the Cassie–Baxter and Wenzel states could coexist.[11,17−28] These two states are separated by an energy barrier, which prevents a droplet from completely wetting the surface.[23−27] Therefore, to drive droplet irreversibly

Received: November 20, 2014
Revised: January 15, 2015

DOI: 10.1021/la5045442
Langmuir XXXX, XXX, XXX–XXX

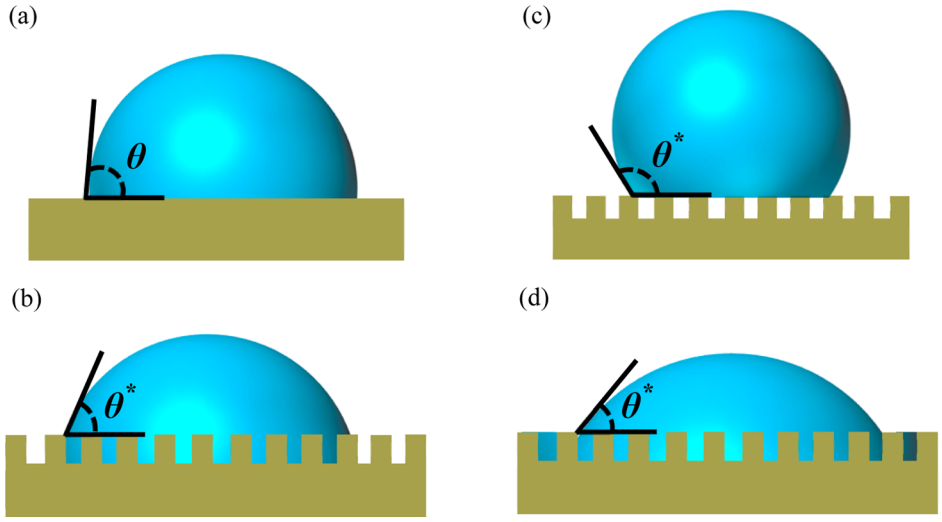

Figure 1. Schematic representation of the droplet on smooth substrate (a), in the Wenzel's state (b), in the Cassie–Baxter's state (c), and in the Cassie impregnating state (d).

from the Cassie–Baxter state to the Wenzel state, it is required to apply an external stimuli.[17,23]

In the Cassie impregnating state, a liquid covers the surface texture such that a droplet resides on top of the solid/liquid composite surface (see Figure 1d).[15,16] The apparent contact angle θ^* in this state is given by the following expression:

$$\cos\theta^* = (1 - f_S) + f_S \cos\theta \tag{2b}$$

It follows from this equation that the spreading of the liquid film beyond the drop smoothens the substrate roughness and improves substrate wetting properties, $\theta^* < \theta$. The Cassie impregnating state is also separated by an energy barrier from the Wenzel state.[15,16]

It is important to point out that eqs 1 and 2 break down when the droplet contact area becomes comparable to the characteristic size of the pattern features covering a substrate.[29,30]

In the case of the elastic solids, due to the surface roughness the real contact area is only a fraction of the nominal contact area.[31−36] Greenwood and Williamson[31] described a rough surface as made of spherical bumps of equal radius, the height of which followed the Gaussian distribution. This model predicts that the contact area A is nearly proportional to the applied load, F_N. Note that for Hertzian-like contact the contact area A scales with applied load as $F_N^{2/3}$.[37] The model extension, which takes into account adhesion between elastic solids and hard rough surfaces, was proposed by Fuller and Tabor.[31] Persson et al.[32,33] have described the surface roughness by a self-affine fractal and observed a full contact when the fractal dimension is below 2.5. When the fractal dimension becomes larger than 2.5, the contact area and the adhesion forces start to decrease dramatically.

In the above examples, wetting and adhesion phenomena have long been considered as two separate cases of interactions with substrates. However, recent studies have shown that the contact phenomena on micro- and nanoscales are governed by a fine interplay between elastic and capillary forces.[38−44] In particular, it was demonstrated that for soft particles the equilibrium contact area with a rigid substrate is controlled by the work of adhesion of nanoparticle to a substrate, elastic energy of particle deformation, and nanoparticle surface free energy due to its shape variation upon adhesion.[39] According to this model for soft particles with size R_p, shear modulus G_p, surface tension γ_p, and work of adhesion W between particle and substrate, there exists a dimensionless parameter $\gamma_p(G_pR_p)^{-2/3}W^{-1/3}$, which describes crossover between adhesion and wetting regimes. Note that for the majority of soft elastic solids, this parameter is on the order of unity. Therefore, to describe interactions of such particles with adhesive substrates, one has to take into account all three contributions.

In this Article, we use a combination of molecular dynamics simulations and analytical calculations to study interactions of soft nanoparticles with patterned surfaces. In particular, we will show that an increase in nanoparticle shear modulus changes the affinity between nanoparticle and substrate, making the substrate more nanoparticle-phobic and stabilizing the Cassie–Baxter state. The rest of this Article is organized as follows. Section 2 discusses model and simulation details. In section 3, we present our simulation results. Derivation of a scaling model of particle interactions with patterned surfaces and model comparison with simulation results are summarized in section 4.

2. MODEL AND SIMULATION DETAILS

We have performed coarse-grained molecular dynamics simulations of adhesion of elastic spherical nanoparticles on patterned surfaces (see Figure 2a). The spherical nanoparticles with radius R_p were made by cross-linking bead–spring chains with the number of monomers (beads) $N = 32$. The elastic modulus of nanoparticles was controlled by changing cross-linking density ρ_c between chains. In our simulations, we used nanoparticles with radius R_p varying between 10.34σ and 34.55σ and having shear modulus changing between $0.023k_BT/\sigma^3$ and $0.853k_BT/\sigma^3$ (where σ is the bead diameter, k_B is the Boltzmann constant, and T is the absolute temperature). The details of the nanoparticle preparation procedure are described in refs 39 and 40.

We studied interactions of these nanoparticles with patterned substrates having postlike patterns (Figure 2). Each post was made of n_{sub} layers of beads with diameter σ that were arranged into hexagonal closed-packed lattice with a number density $1.0\sigma^{-3}$. The pattern dimensions are characterized by the width

DOI: 10.1021/la5045442
Langmuir XXXX, XXX, XXX−XXX

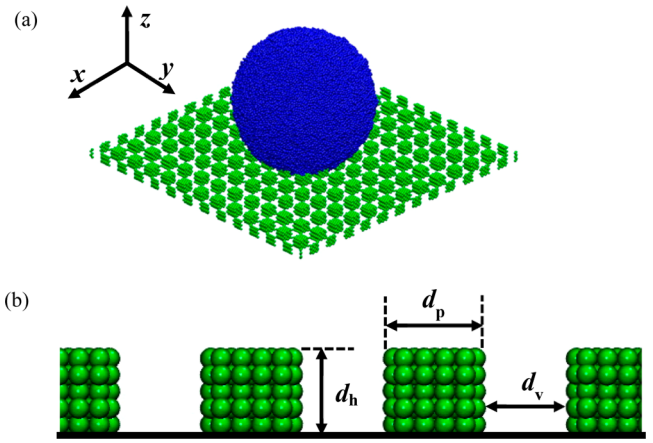

Figure 2. Snapshot of the simulation box containing nanoparticle and textured substrate with postlike grid pattern (a) with dimensions d_p, d_h, and d_v (b).

d_p, height d_h, and spacing d_v as shown in Figure 2b. Parameters of the substrate patterns used in simulations are listed in Table 1. The posts were placed on top of an attractive rigid substrate modeled by the effective external potential (see discussion below).

Table 1. Dimensions of Textured Substrates

n_{sub}	d_h [σ]	d_v [σ]	d_p [σ]
3	2.83	2.5	2.5
5	4.67	5.0	5.0

In our simulations, the interactions between all beads in a system were modeled by the truncated-shifted Lennard-Jones (LJ) potential:[45]

$$U_{LJ}(r_{ij}) = \begin{cases} 4\varepsilon_{LJ}\left[\left(\frac{\sigma}{r_{ij}}\right)^{12} - \left(\frac{\sigma}{r_{ij}}\right)^{6} - \left(\frac{\sigma}{r_{cut}}\right)^{12} + \left(\frac{\sigma}{r_{cut}}\right)^{6}\right] & r \le r_{cut} \\ 0 & r > r_{cut} \end{cases} \quad (3)$$

where r_{ij} is the distance between the ith and jth beads and σ is the bead diameter. The values of the cutoff distance r_{cut} and the values of the Lennard-Jones interaction parameters ε_{LJ} are summarized in Table 2 in terms of the thermal energy k_BT. The connectivity of the beads into polymer chains and the cross-link bonds were modeled by the finite extension nonlinear elastic (FENE) potential:[46]

Table 2. Interaction Parameters

	weak interactions			strong interactions		
	NP−NP	NP−post	NP−sub	NP−NP	NP−post	NP−sub
ε [k_BT]	1.5	0.71	1.5	1.5	1.42	3.0
r_{cut} [σ]	2.5	5.0		2.5	5.0	

$$U_{FENE}(r) = -\frac{1}{2}k_{spring}R_{max}^2 \ln\left(1 - \frac{r^2}{R_{max}^2}\right) \quad (4)$$

with the spring constant $k_{spring} = 30k_BT/\sigma^2$ and the maximum bond length $R_{max} = 1.5\sigma$. The repulsive part of the bond potential was modeled by the LJ-potential with $r_{cut} = 2^{1/6}\sigma$ and $\varepsilon_{LJ} = 1.5k_BT$.

The attractive solid substrates were modeled by the effective external potential:

$$U(z) = \varepsilon_w\left[\frac{2}{15}\left(\frac{\sigma}{z}\right)^9 - \left(\frac{\sigma}{z}\right)^3\right] \quad (5)$$

where ε_w was set to $1.5k_BT$ and $3.0k_BT$. The long-range attractive part of the potential z^{-3} represents the effect of van der Waals interactions generated by the wall half-space.

The system was periodic in x and y directions with dimensions $L_x = L_y = L_z = 4.0R_0$ where R_0 is the radius of the confining cavity used for nanoparticle preparation.[39]

Simulations were carried out in a constant number of beads and temperature ensemble. The constant temperature was maintained by coupling the system to a Langevin thermostat.[45] In this case, the equation of motion of the ith bead belonging to nanoparticle is

$$m\frac{d\vec{v}_i(t)}{dt} = \vec{F}_i(t) - \xi\vec{v}_i(t) + \vec{F}_i^R(t) \quad (6)$$

where m is the bead mass set to unity for all beads in a system, $\vec{v}_i(t)$ is the bead velocity, and $\vec{F}_i(t)$ is the net deterministic force acting on the ith bead. The stochastic force $\vec{F}_i^R(t)$ has a zero average value and δ-functional correlations $\langle\vec{F}_i^R(t)\cdot\vec{F}_i^R(t')\rangle = 6k_BT\xi(t - t')$. The friction coefficient ξ was set to $\xi = m/\tau_{LJ}$, where τ_{LJ} is the standard LJ-time $\tau_{LJ} = \sigma(m/\varepsilon_{LJ})^{1/2}$. The velocity-Verlet algorithm with a time step $\Delta t = 0.01\tau_{LJ}$ was used for integration of the equation of motion. All simulations were performed using LAMMPS.[47] Note that the locations of beads forming posts were fixed. This reduced presence of the substrate features to the effective external potential. At the beginning of each simulation, the center mass of a nanoparticle was placed at a distance $R_p + 2.0\sigma$ from the top of the substrate pattern. The system was equilibrated for $4 \times 10^4\tau_{LJ}$ followed by the production run lasting $10^4\tau_{LJ}$.

The surface tension of the nanoparticle, γ_p, was obtained from simulations of the gel-like films having the same interaction parameters and cross-linking density as nanoparticles. In these simulations, the surface tension is evaluated from integration of difference of the normal $P_N(z)$ and tangential $P_T(z)$ to the interface components of the pressure tensor (see refs 39 and 44 for detail). The shear modulus of nanoparticles as a function of the cross-linking density was obtained from 3-D simulations of bulk gel sample with the same cross-linking density and interaction parameters.[39,40] In our simulations, we covered the range of nanoparticle surface tensions γ_p between $1.84k_BT/\sigma^2$ and $2.4k_BT/\sigma^2$.

Work of adhesion between nanoparticle and substrate was evaluated from the potential of mean force between substrate and gel film. In these simulations, a gel film with initial dimensions $20\sigma \times 20\sigma \times 15\sigma$ was pushed toward a substrate. We performed two different types of simulations. In the first type of simulation, the gel was interacting with a patterned substrate, while in the second type of simulation, layers of beads were covering the whole substrate without patterns. The location of the substrate was fixed. In these simulations, the

DOI: 10.1021/la5045442
Langmuir XXXX, XXX, XXX−XXX

center of mass of the gel-like film, z_{cm}, was tethered at z^* by a harmonic potential:

$$U(z_{cm}, z^*) = \frac{1}{2}K_{sp}(z_{cm} - z^*)^2 \quad (7)$$

with the value of the spring constant $K_{sp} = 1000k_BT/\sigma^2$. The location of the film's tethering point was moved with an increment $\Delta z^* = 0.1\sigma$ toward substrate. For each location of the tethering point, we have performed a simulation run lasting $5 \times 10^3\tau_{LJ}$, during which we have calculated distribution of the center of mass of the gel film. The weighted histogram analysis method (WHAM)[48] was applied to calculate potential of the mean force between gel film and substrate from distribution functions of the film center of mass. Table 3 summarizes our results for the work of adhesion, $W = \Delta F/A$, as a function of the interaction parameters, substrate structure, and the cross-linking density of the gel films.

Table 3. Work of Adhesion W $[k_BT/\sigma^2]$

			G_p $[k_BT/\sigma^3]$					
n_{sub}	ε_{sp} $[k_BT]$	ε_{wp} $[k_BT]$	0.023	0.096	0.212	0.375	0.588	0.853
			W_{sp}					
3	0.71	1.50	1.61	1.68	1.72	1.76	1.85	1.89
3	1.42	3.00	3.25	3.60	4.11	4.30	4.61	4.71
5	0.71	1.50	1.60	1.64	1.69	1.76	1.83	1.88
5	1.42	3.00	3.21	3.54	4.04	4.18	4.50	4.63
			W_{wp}					
0	0	1.50	1.04	1.06	1.07	1.08	1.10	1.12
0	0	3.00	2.09	2.12	2.14	2.17	2.20	2.24
			Patterned Substrates					
			G_p $[k_BT/\sigma^3]$					
n_{sub}	ε_{sp} $[k_BT]$	ε_{wp} $[k_BT]$	0.023	0.096	0.212	0.375	0.588	0.853
3	0.71	1.50	0.72	0.68	0.65	0.61	0.60	0.59
3	1.42	3.00	2.27	2.71	3.03	3.20	2.87	2.37
5	0.71	1.50	0.60	0.47	0.49	0.54	0.54	0.55
5	1.42	3.00	2.63	3.04	3.17	2.22	1.61	1.45

In our simulations, we used a coarse-grained representation of studied systems and expressed the strength of interactions in terms of the thermal energy k_BT. (Note that in such a representation the relative magnitude of the interaction parameters controls wetting and adhesion of nanoparticles.) To map our coarse-grained system representation into a real system at T = 300 K, we will use the surface tension of nanoparticle as a mapping quantity. For example, let's assume that our nanoparticles are made of cross-linked PDMS, which has a surface tension on the order of 21 mN/m.[1] Using this value for surface tension of nanoparticle with the lowest cross-linking density $\gamma_p = 1.84k_BT/\sigma^2$, we can solve for the bead size σ = 0.6 nm. For such bead sizes, the nanoparticle shear modulus G_p is varied between 0.4 and 16 MPa, and the work of adhesion is between 5.4 and 54 mN/m (see Table 3).

3. SIMULATION RESULTS

In Figure 3, we show evolution of nanoparticle shape deformation and contact with substrate for nanoparticles with preparation radius $R_0 = 31.8\sigma$ on surfaces with postlike patterns. As one can see in Figure 3a and b, both tall and short posts penetrate soft nanoparticles such that the contact between nanoparticles and substrates can be viewed as the Wenzel state. However, with increasing nanoparticle elastic modulus, the interaction between substrate and nanoparticle is weakened, resulting in crossover to Cassie−Baxter-like contact between nanoparticle and system of posts. The gap between nanoparticle and substrate is larger for the system of taller posts (Figure 3c) in comparison with that for the system of shorter posts (Figure 3d). Therefore, both amplitude of the surface roughness and nanoparticle elastic properties influence crossover between Wenzel and Cassie−Baxter states, making the substrate effectively more nanoparticle phobic.

Figures 4a−c shows how the transition between Wenzel and Cassie−Baxter states for nanoparticles of different sizes and gel film depends on the strength of interactions, post height, and shear modulus. For short posts, n_{sub} = 3 (see Figure 4a), and the strongest nanoparticle−substrate interactions, $\varepsilon_{sp} = 1.42k_BT$, there is no dependence of the depth of indentations produced by substrate posts in the foot of nanoparticle on nanoparticle size. All data points group together. However, indentation depth δ slowly decreases with increasing nanoparticle shear modulus, $\tilde{G}_p$, indicating that an equilibrium depth of indentation is a result of a fine interplay between attraction of nanoparticle to substrate and elastic deformation of nanoparticle foot. This observation is further corroborated by

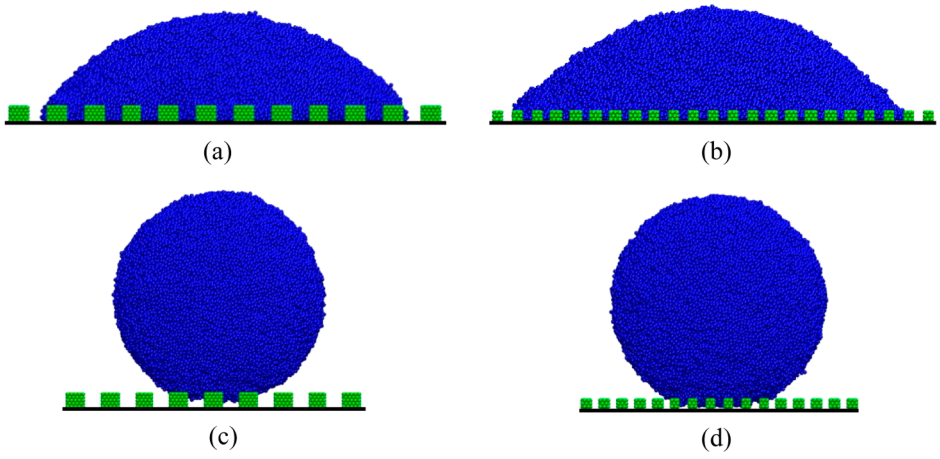

Figure 3. Snapshots of deformation of nanoparticle with radius $R_0 = 31.8\sigma$ on textured substrates: (a) n_{sub} = 5, $G_p = 0.023k_BT/\sigma^3$, $\varepsilon_{sp} = 1.42k_BT$; (b) n_{sub} = 3, $G_p = 0.023k_BT/\sigma^3$, $\varepsilon_{sp} = 1.42k_BT$; (c) n_{sub} = 5, $G_p = 0.853k_BT/\sigma^3$, $\varepsilon_{sp} = 0.71k_BT$; (d) n_{sub} = 3, $G_p = 0.853k_BT/\sigma^3$, $\varepsilon_{sp} = 0.71k_BT$.

DOI: 10.1021/la5045442
Langmuir XXXX, XXX, XXX−XXX

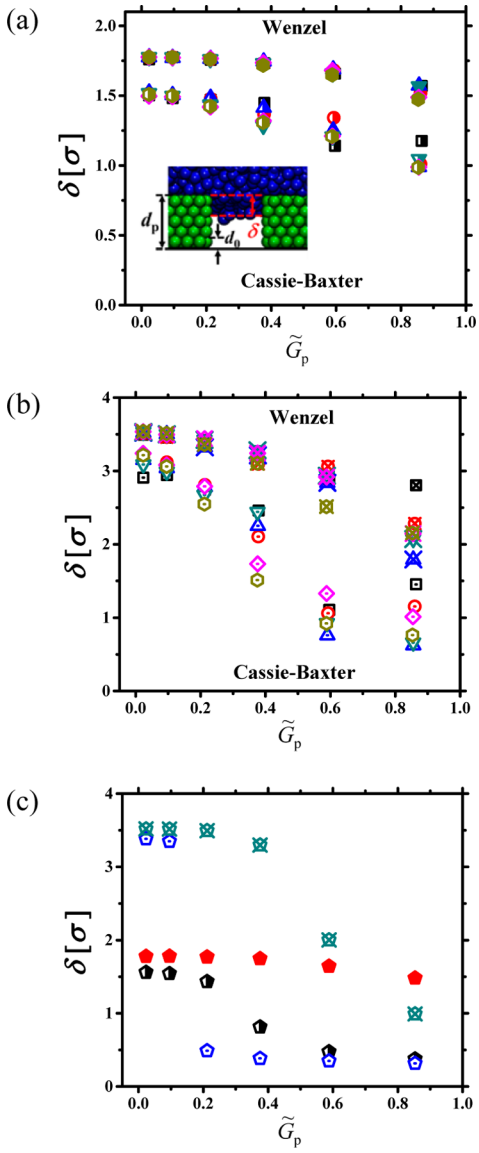

Figure 4. Dependence of the indentation depth δ on the nanoparticle shear modulus $\tilde{G}_p = G_p\sigma^3/k_BT$ for nanoparticles of different sizes R_0, 11.3σ (black squares), 16.4σ (red circles), 20.5σ (blue triangles), 26.7σ (cyan inverted triangles), 31.8σ (magenta diamonds), 36.0σ (yellow hexagons), interacting with patterned substrates: (a) n_{sub} = 3, ε_{sp} = 0.71k_BT (half-filled symbols); n_{sub} = 3, ε_{sp} = 1.42k_BT (filled symbols); and (b) n_{sub} = 5, ε_{sp} = 0.71k_BT (centered dot symbols); n_{sub} = 5, ε_{sp} = 1.42k_BT (crossed open symbols). Inset in (a) shows definition of the length scales, and d_0 = 0.867σ is the distance of the closest approach between center of mass of beads forming nanoparticle in the substrate external potential. (c) Dependence of the equilibrium indentation depth δ on the gel shear modulus $\tilde{G}_p = G_p\sigma^3/k_BT$ obtained from WHAM simulations of substrate−gel interactions for patterned surfaces: n_{sub} = 3, ε_{sp} = 0.71k_BT (black half-filled pentagons); n_{sub} = 3, ε_{sp} = 1.42k_BT (red filled pentagons); n_{sub} = 5, ε_{sp} = 0.71k_BT (blue centered dot pentagons); n_{sub} = 5, ε_{sp} = 1.42k_BT (crossed cyan open pentagons).

the decrease in the magnitude of indentations produced by posts in nanoparticles for systems with weaker nanoparticle−substrate interactions, ε_{sp} = 0.71k_BT. Note that for these systems, we also start to see dependence of indentation δ on nanoparticle sizes as nanoparticle shear modulus increases. It is also important to point out that for all systems with short posts, contact of nanoparticle with substrate is closer to the Wenzel state rather than to the Cassie−Baxter state. The situation changes for systems with larger posts, n_{sub} = 5, as shown in Figure 4b. For these systems, we observe a stronger dependence of indentation on the nanoparticle sizes. The strongest dependence is seen for more rigid nanoparticles that are in the Cassie−Baxter state. In this case, smaller nanoparticles reside between the posts. Such contact with substrate maximizes nanoparticle attraction to the substrate and at the same time minimizes its elastic energy penalty. Furthermore, for systems of nanoparticles with ε_{sp} = 0.71k_BT, we observe an abrupt transition between Wenzel and Cassie−Baxter states with increasing nanoparticle shear modulus. However, for nanoparticles with ε_{sp} = 1.42k_BT, the indentation depth δ gradually decreases with increasing nanoparticle shear modulus. This could be explained by coexistence of the Wenzel and Cassie−Baxter states in the nanoparticle contact area. To elucidate finite size effects on the transition between the Wenzel and Cassie−Baxter states in Figure 4c, we show simulation results for interaction of patterned substrates with gel films. The sharp transition between Wenzel and Cassie−Baxter states with increasing gel shear modulus is observed for systems with ε_{sp} = 0.71k_BT and n_{sub} = 5. However, for the systems with the same post height but with stronger gel−substrate interactions, ε_{sp} = 1.42k_BT, the transition between Wenzel and Cassie−Baxter states looks more like a crossover. Such a peculiar dependence of the contact structure on the system parameters could be a manifestation of the first-order type transition between Wenzel and Cassie−Baxter states. In this case, the average value of the indentation depth δ plotted in Figure 4a−c is a result of sampling between the Wenzel state and the Cassie−Baxter states in the interval of parameters where both states coexist.

Figure 5 shows the free energy change of small nanoparticles calculated by using WHAM[48] as they contact a patterned substrate. This figure clearly shows the existence and coexistence of two different states for nanoparticles in contact with patterned surfaces. Therefore, for the elastic nanoparticles interacting with patterned substrates, the transition between the

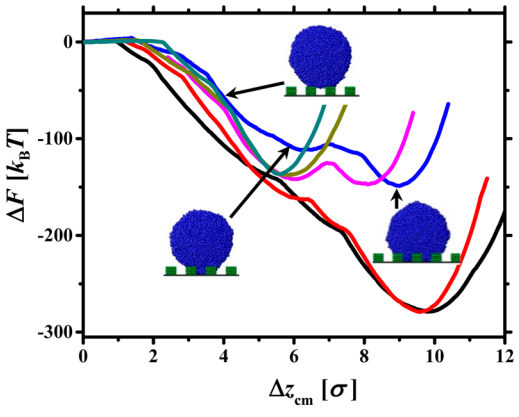

Figure 5. Free energy change ΔF of nanoparticle with R_0 = 16.4σ obtained from WHAM simulations of gel slabs with values of the shear modulus G_p = 0.023k_BT/σ^3 (black line), G_p = 0.096k_BT/σ^3 (red line), G_p = 0.214k_BT/σ^3 (blue line), G_p = 0.379k_BT/σ^3 (pink line), G_p = 0.596 k_BT/σ^3 (dark yellow line), and G_p = 0.863k_BT/σ^3 (cyan line) interacting with patterned substrates having n_{sub} = 5 and values of the interaction parameter ε_{sp} =1.42k_BT. Insets show typical nanoparticle conformations.

DOI: 10.1021/la5045442
Langmuir XXXX, XXX, XXX−XXX

Wenzel and Cassie–Baxter states is a first-order transition. This situation is similar to a wetting transition of liquid droplets on patterned surfaces.[23−27]

In addition to controlling crossover between Wenzel and Cassie–Baxter states, nanoparticle elasticity and strength of nanoparticle–substrate interactions are also responsible for nanoparticle shape deformation. To elucidate these effects and to establish that our nanoparticles are soft enough to demonstrate both adhesive and wetting behavior, in Figure 6

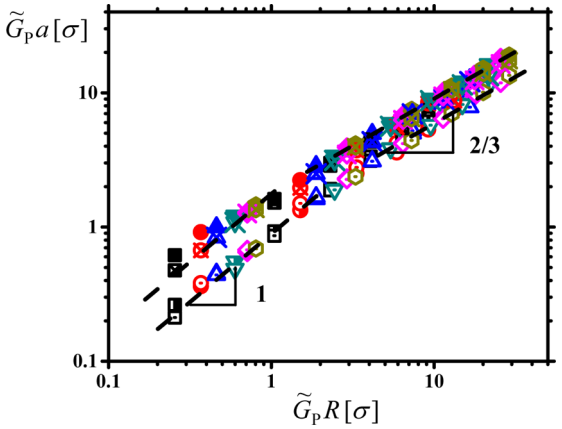

Figure 6. Comparison of simulation results with JKR model for nanoparticles of different sizes R_p and different values of shear modulus $\tilde{G}_p = G_p\sigma^3/k_BT$ adsorbed on patterned substrates. Notations are the same as in Figure 4a and b.

we show deviation of the nanoparticle contact radius, a, from Johnson, Kendall, and Roberts (JKR) scaling.[31,37] For adhesive contact between elastic nanoparticle with modulus G_p and radius R_p and solid substrate, the equilibrium contact radius a of nanoparticle with substrate is expected to have the following scaling dependence on the particle size $aG_p \propto (G_pR_p)^{2/3}$.[37] This scaling relation is obtained by balancing the elastic energy of nanoparticle deformation $U_{el} \propto G_pa^5/R_p^2$ and work of adhesion πa^2W.[37] For rigid nanoparticles, we observe the expected scaling relationship (see Figure 6). However, for soft nanoparticles, our data sets demonstrate linear scaling, $a \propto R_p$. Note that the observed linear scaling dependence is a characteristic feature of dominance of the capillary forces over nanoparticle elasticity in controlling its shape. It is interesting to point out that the data corresponding to strong and weak nanoparticle–substrate interactions are shifted with respect to each other, thus pointing out that the work of adhesion is proportional to the magnitude of the interaction potentials. Below we will develop a scaling model that accounts for both elastic and capillary forces contributions into deformation of a nanoparticle in contact with a patterned surface.

4. MODEL OF NANOPARTICLE INTERACTION WITH PATTERNED SUBSTRATE

We will follow our previous work[39,44] and approximate the shape of the deformed nanoparticle of size R_p by a spherical cap with height h and contact radius a (see Figure 7). The radius of curvature of the spherical cap is equal to R_1. The change in the total free energy of nanoparticle upon contact with substrate has elastic energy and surface energy contributions. We first evaluate elastic energy of the deformed nanoparticle. There are two elastic energy contributions due to deformation of nanoparticle on textured surfaces: (i) elastic energy contribu-

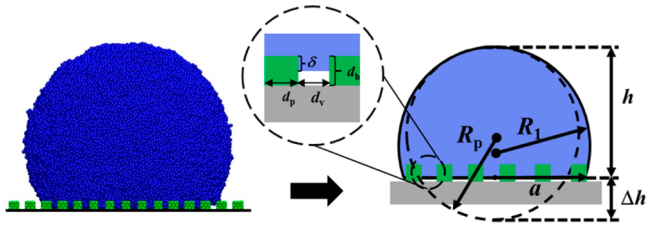

Figure 7. Schematic representation of nanoparticle shape deformation upon contact with a patterned substrate.

tion due to macroscopic shape deformation of nanoparticles and (ii) elastic energy contribution due to indentations of depth δ produced by the substrate posts in the nanoparticle within a contact area πa^2. For nanoparticle height deformation $\Delta h = 2R_p - h$, the value of the restoring stress σ_{zz} acting in the contact area due to nanoparticle height deformation is on the order of $G_p\Delta h/a$. This stress is distributed over area πa^2 producing a restoring force on the order of $\sigma_{zz}a^2$. The elastic energy of nanoparticle shape deformation is on the order of the work required to maintain height deformation Δh with a force equal to a restoring force $\sigma_{zz}a^2$. This results in the elastic energy of the nanoparticle shape deformation to be on the order of

$$U_{elast}^{sh} \propto \sigma_{zz}a^2\Delta h \approx G_p\Delta h^2 a \tag{8}$$

The elastic energy contribution generated by each post can be estimated by using similar scaling arguments. Indentation of depth δ produced by a post in a foot of nanoparticle generates a restoring stress on the order of $G_p\delta/d_p$. This stress produces a restoring force $d_p^2G_p\delta/d_p \approx G_p\delta d_p$. Therefore, the elastic energy due to indentation produced by each post can be estimated as $G_p\delta^2d_p$. There are $\pi a^2/(d_p + d_v)^2$ posts within a contact area, πa^2. Combining contributions from all posts, we obtain:

$$U_{elast}^{post} \propto G_p\delta^2 d_p a^2/(d_p + d_v)^2 \approx \alpha G_p\delta^2 a^2/d_p \tag{9}$$

where we introduced parameter $\alpha = d_p^2/(d_v + d_p)^2$, the fraction of the surface occupied by the posts. Adding two terms together, we can write the expression for the total elastic energy of the nanoparticle interacting with patterned substrate:

$$U_{elast} \propto G_p\Delta h^2 a + \alpha G_p\delta^2 a^2/d_p \tag{10}$$

The surface free energy of deformed nanoparticle of height h and radius R_1 in contact with patterned substrate of surface area A can be written as follows:

$$F_{surf}(a, h, \delta) = (A - \pi a^2)\left(\alpha\gamma_s + (1 - \alpha)\gamma_w + \frac{4d_h\alpha}{d_p}\gamma_s\right) + \pi a^2\left((1 - \alpha)\left(\gamma_p + \gamma_w - W_{wp}\frac{f(d_h - \delta)}{f(d_0)}\right) + \alpha\gamma_{sp} + \frac{4\alpha\delta}{d_p}\gamma_{sp} + \frac{4\alpha(d_h - \delta)}{d_p}\gamma_s\right) + 2\pi R_1h\gamma_p \tag{11}$$

The first term on the right-hand side of eq 11 describes the contribution from the surface of the substrate with surface area $A - \pi a^2$ and surface tensions γ_s of the post surface and γ_w of the rigid half-space described by the external potential given in eq 5. The second term accounts for the surface free energy due to surface area of the contact between nanoparticle and patterned substrate with surface tension γ_p and nanoparticle/substrate

DOI: 10.1021/la5045442
Langmuir XXXX, XXX, XXX−XXX

surface tension γ_{sp}, and the last term corresponds to the surface free energy contribution from the exposed area of nanoparticle $2\pi R_1 h$ with surface tension γ_p. In eq 11, we have introduced work of adhesion, $W_{wp} = \gamma_w + \gamma_p - \gamma_{wp}$ (where γ_{wp} is the nanoparticle−rigid wall surface tension). Function

$$f(z) = \frac{1}{2}\left(\frac{\sigma}{z}\right)^2 - \frac{1}{60}\left(\frac{\sigma}{z}\right)^8 \tag{12}$$

takes into account the long-range van der Waals interactions between rigid half-space and nanoparticle and is obtained by integration of the z-dependent part of the interaction potential eq 5. For interaction potential eq 5, the work of adhesion between nanoparticle and rigid wall is evaluated as $W_{wp} = 0.622\varepsilon_w\rho_p\sigma$ where ρ_p is the monomer density inside the nanoparticle. Note that complete contact between nanoparticle and substrate (Wenzel state) occurs for indentation depth $\delta = d_h - d_0$. In this case, interaction between nanoparticle and rigid wall reduces to $\gamma_p + \gamma_w - W_{wp} = \gamma_{wp}$.

We can eliminate radius of curvature of the deformed nanoparticle R_1 by using the geometric relation between contact radius a and nanoparticle height h:

$$R_1^2 = a^2 + (h - R_1)^2 \tag{13}$$

Solving this equation for hR_1 and substituting this solution into eq 11, we obtain:

$$F_{surf}(a, h, \delta) = A\left(\gamma_s + \frac{4d_h\alpha}{d_p}\gamma_s\right) + \pi a^2\left(2\gamma_p - \left(\alpha W_{sp} + (1-\alpha)W_{wp}\frac{f(d_h-\delta)}{f(d_0)}\right) + \frac{4\alpha\delta}{d_p}(\gamma_{sp} - \gamma_s)\right) + \pi h^2\gamma_p \tag{14}$$

where work of adhesion $W_{sp} = \gamma_s + \gamma_p - \gamma_{sp}$. Because the elastic energy of nanoparticle deformation eq 10 is expressed in terms of Δh, a, and δ, it is convenient to describe nanoparticle surface free energy using similar variables. Taking this into account, we can rewrite eq 14 as follows:

$$F_{surf}(a, \Delta h, \delta) = A\left(\gamma_s + \frac{4d_h\alpha}{d_p}\gamma_s\right) + 4\pi R_p^2\gamma_p + \pi a^2\left(2\gamma_p - \left(\alpha W_{sp} + (1-\alpha)W_{wp}\frac{f(d_h-\delta)}{f(d_0)}\right) + \frac{4\alpha\delta}{d_p}(\gamma_{sp} - \gamma_s)\right) - 4\pi R_p\Delta h\gamma_p + \pi\Delta h^2\gamma_p \tag{15}$$

The change of the system surface free energy upon contact of a nanoparticle with the substrate is equal to

$$\Delta F_{surf}(a, \Delta h, \delta) = F_{surf}(a, \Delta h, \delta) - F_{surf}(0, 0, 0) = \pi a^2\left(2\gamma_p - \left(\alpha W_{sp} + (1-\alpha)W_{wp}\frac{f(d_h-\delta)}{f(d_0)}\right) + \frac{4\alpha\delta}{d_p}(\gamma_{sp} - \gamma_s)\right) - 4\pi R_p\Delta h\gamma_p + \pi\Delta h^2\gamma_p \tag{16}$$

For elastomeric nanoparticles, their deformation occurs at a constant volume. Thus, there are only two independent parameters describing nanoparticle shape deformation. Here, we will assume that indentation δ is smaller than Δh such that post contribution can be neglected in the evaluation of the volume of deformed nanoparticle. Taking this into account, the volume conservation condition has the following form:

$$\frac{4\pi}{3}R_p^3 = \pi\left(R_1h^2 - \frac{h^3}{3}\right) \tag{17}$$

In the limit of small nanoparticle deformations, $\Delta h/2R_p \ll 1$, from eq 17 we obtain $a^2 \approx 2R_p\Delta h$. Substituting this relation into eq 16, we can rewrite the change in the surface free energy of nanoparticle upon contact with patterned substrate as a function of Δh and δ:

$$\Delta F_{surf}(\Delta h, \delta) \approx -2\pi R_p\Delta h\left(\alpha W_{sp} + (1-\alpha)W_{wp} \times \frac{f(d_h-\delta)}{f(d_0)} + \frac{4\alpha\delta}{d_p}(W_{sp} - \gamma_p)\right) + \pi\Delta h^2\gamma_p \tag{18}$$

Finally, by combining the elastic (eq 10) and surface (eq 18) free energy terms, we arrive at the expression describing deformation of elastic nanoparticle on rigid patterned substrate:

$$\Delta F(\Delta h, \delta) \approx C_G G_p R_p^{1/2}\Delta h^{5/2} + \pi\Delta h^2\gamma_p - 2\pi R_p\Delta h W_{eff}(\delta) \tag{19}$$

where C_G is numerical constant, and we introduced effective work of adhesion:

$$W_{eff}(\delta) = \alpha W_{sp} + (1-\alpha)W_{wp}\frac{f(d_h-\delta)}{f(d_0)} + \frac{4\alpha\delta}{d_p}(W_{sp} - \gamma_p) - \frac{C_p}{2\pi}\frac{\alpha G_p\delta^2}{d_p} \tag{20}$$

which depends on the contact between nanoparticle and substrate (C_p is a numerical constant). Equation 19 generalizes our result[39,44] to the case of nanoparticle interaction with patterned surfaces. The equilibrium nanoparticle height deformation Δh and indentation δ produced by substrate posts in nanoparticle foot can be obtained by minimizing the nanoparticle free energy eq 18.

We will first analyze the behavior of function $W_{eff}(\delta)$ to describe the transition between the Cassie−Baxter and Wenzel states. Figure 8 shows the evolution of function $-W_{eff}(\delta)$ for nanoparticles with different values of the shear modulus adsorbed on substrates covered with post consisting of five layers of beads. It follows from this figure that there are two different states characterizing interaction of the nanoparticle with substrate. The first state corresponds to the Cassie−Baxter state ($\delta = 0$) when the nanoparticle resides on top of the posts, and the second one describing a nanoparticle in contact with rigid wall corresponds to the Wenzel state. For rigid nanoparticles with $G_p > 0.4k_BT/\sigma^3$, the Cassie−Baxter state is the lowest free energy state. Note that at these values of the shear modulus, the Wenzel state still exists and is metastable. As the value of the shear modulus decreases, the Wenzel state becomes a thermodynamically stable state with a contact free energy lower than that of the Cassie−Baxter state. Finally, for

DOI: 10.1021/la5045442
Langmuir XXXX, XXX, XXX−XXX

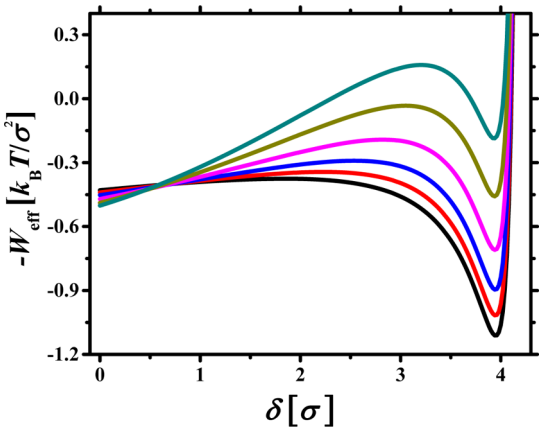

Figure 8. Contact free energy $-W_{eff}(\delta)$ obtained from eq 20 with value of the numerical $C_p = 2\pi$ for nanoparticles with values of the shear modulus $G_p = 0.023k_BT/\sigma^3$ (black line), $G_p = 0.096k_BT/\sigma^3$ (red line), $G_p = 0.214k_BT/\sigma^3$ (blue line), $G_p = 0.379k_BT/\sigma^3$ (pink line), $G_p = 0.596k_BT/\sigma^3$ (dark yellow line), and $G_p = 0.863k_BT/\sigma^3$ (cyan line) adsorbed on patterned substrates with $n_{sub} = 5$ and values of the interaction parameter $\varepsilon_{sp} = 1.42k_BT$.

very soft nanoparticles, the Wenzel state becomes the only equilibrium state with the lowest free energy of contact. Thus, in the framework of our simple scaling model, the transition between the Cassie−Baxter and Wenzel states is a first-order transition. To test that this is indeed the case, in Figure 9 we

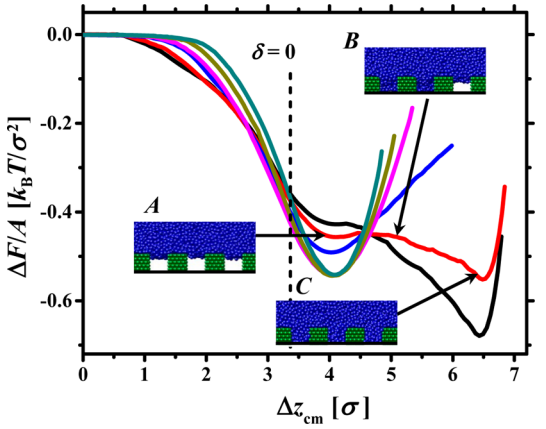

Figure 9. Contact free energy per unit area $\Delta F/A$ obtained from WHAM simulations of gel slabs with values of the shear modulus $G_p = 0.023k_BT/\sigma^3$ (black line), $G_p = 0.096k_BT/\sigma^3$ (red line), $G_p = 0.214k_BT/\sigma^3$ (blue line), $G_p = 0.379k_BT/\sigma^3$ (pink line), $G_p = 0.596k_BT/\sigma^3$ (dark yellow line), and $G_p = 0.863k_BT/\sigma^3$ (cyan line) interacting with patterned substrates having $n_{sub} = 5$ and values of the interaction parameter $\varepsilon_{sp} = 1.42k_BT$. Insets show typical gel conformations.

show results of the WHAM calculations of the potential of the mean force between patterned substrate and a gel film. Simulations of the gel film allowed us to eliminate contribution coming from the nanoparticle shape deformation as it wets the substrate. It is important to point out that our model of the contact between nanoparticle foot and a substrate assumes that particle size does not influence the structure of the contact layer. This effectively corresponds to adhesive contact between patterned substrate and infinite gel, which has the same characteristics as a gel-forming nanoparticle. The free energy curves shown in Figure 9 confirm the existence of the transition between Cassie−Baxter and Wenzel states. For rigid gels with $G_p \geq 0.214k_BT/\sigma^3$, the contact free energy has a minimum when gel touches the substrate. However, for softer gels, we observe the existence of two states: one corresponding to gel residing on the top of the substrate pattern (Cassie−Baxter state) and another corresponding to a complete contact with substrate pattern (Wenzel state). In the range of displacements of the gel center of mass Δz_{cm} between these two states, there is a coexistence of the Cassie−Baxter and Wenzel states with part of the gel being in the Cassie−Baxter state and the other part being in Wenzel state. The coexistence of two states is also supported by the probability distribution of the indentation depth δ shown in Figure 10.

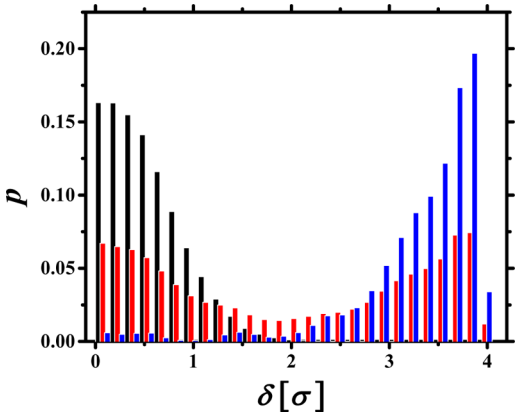

Figure 10. Distribution function of the indentation depth δ as a function of the gel center of mass displacement for three different center of mass displacements as shown in Figure 9. Black, red, and blue bars correspond to locations A, B, and C shown in Figure 9, respectively.

In our analysis of nanoparticle shape deformation described by eq 19, due to interaction with the patterned substrate, we will use the value of W_{eff} obtained from WHAM simulations of gel slab interactions with patterned substrates (see Table 3). This will allow us correctly account for the transition between the Wenzel and Cassie−Baxter states and its effect on nanoparticle shape deformation. The equilibrium height deformation of nanoparticle is obtained by minimizing eq 19 with respect to Δh:

$$0 \approx -2\pi W_{eff} R_p + 2\pi\gamma_p \Delta h + \frac{5}{2} C_G G_p R_p^{1/2} \Delta h^{3/2} \quad (21)$$

It follows from eq 21 that there are two asymptotic solutions describing two different regimes of nanoparticle interaction with substrate.[39,44] In the first regime, nanoparticle deformation is controlled by the adhesion and elastic energy terms (the first and the last terms on the right-hand side of eq 21). In this limit, the solution of eq 21 recovers classical adhesion scaling dependence of the nanoparticle height deformation on the system parameters:[37]

$$\Delta h \propto R_p^{1/3} (W_{eff}/G_p)^{2/3} \quad (22)$$

We called this regime the adhesion regime. In the other asymptotic regime, the equilibrium nanoparticle deformation is obtained by balancing adhesion and surface free energy terms (the first and second terms on the right-hand side of eq 21). This results in the following expression for nanoparticle height deformation:

DOI: 10.1021/la5045442
Langmuir XXXX, XXX, XXX−XXX

$$\Delta h \propto R_p W_{eff}/\gamma_p \tag{23}$$

We called this regime the wetting regime. The crossover between these two regimes occurs at nanoparticle sizes:

$$\tilde{R}_p \propto \frac{\gamma_p^{3/2}}{G_p W_{eff}^{1/2}} \tag{24}$$

Therefore, for small nanoparticles, $R_p < \tilde{R}_p$, the capillary forces control nanoparticle shape, while for large nanoparticles, $R_p > \tilde{R}_p$, nanoparticle elastic energy and its adhesion to the substrate determine nanoparticle deformation. At the crossover, the nanoparticle height deformation is estimated as $\Delta\tilde{h} \propto \gamma_p^{1/2} W_{eff}^{1/2}/G_p$.

We can solve eq 21 for nanoparticle height deformation:[39,44]

$$\frac{\Delta h}{\Delta\tilde{h}} = 2A_G\left(\frac{R_p}{\tilde{R}_p}\right)^{1/3} \times \left(\sqrt[3]{r+\sqrt{q^3+r^2}} + \sqrt[3]{r-\sqrt{q^3+r^2}} - \frac{\beta}{3}\right)^2 \tag{25}$$

where

$$r = \frac{1}{2} - \left(\frac{\beta}{3}\right)^3,\ q = -\left(\frac{\beta}{3}\right)^2,\ \text{and}\ \beta = B_G\left(\frac{\tilde{R}_p}{R_p}\right)^{2/3} \tag{26}$$

and $A_G = (\sqrt{2\pi/5}C_G)^{2/3}$ and $B_G = 2(\sqrt{2\pi/5}C_G)^{2/3}$ are numerical coefficients. Note that the actual values of the parameters A_G and B_G are model dependent, and we will consider them as two adjustable parameters to fit our simulation data.

Figure 11 summarizes our results for nanoparticle deformations on patterned substrates. We have also added to this plot simulation results for nanoparticles interacting with rigid surfaces, rigid nanoparticles interacting with soft substrates, and interactions between nanoparticles and substrates of arbitrary rigidity.[39,44] The data demonstrate a reasonably good collapse indicating that we can use the effective work of adhesion to model interactions between a patterned substrate and a nanoparticle. However, there is a systematic deviation of the data for small nanoparticles, which have parameters corresponding to the crossover region between Cassie–Baxter and Wenzel states. For such nanoparticles, there is a significant difference between values of indentation depths measured for nanoparticles in contact with substrate and those obtained from the gel slab simulations (see Figure 4b). The collapse of the data in the Wenzel regime or pure Cassie–Baxter regime as well as in the crossover regime for our two largest nanoparticles is very good. Therefore, we can conclude that it is possible to use the universal plot shown in Figure 11 and extract optimal values of the work of adhesion, which will collapse small nanoparticle data sets into a universal line. The obtained by this procedure work of adhesion will include corrections due to the finite size effect observed for interaction of small nanoparticles in comparison with those obtained for macroscopic samples.

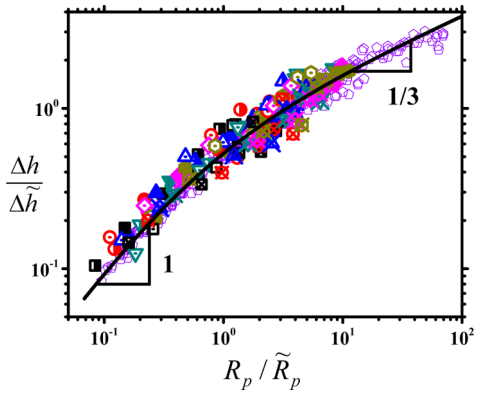

Figure 11. Dependence of the reduced nanoparticle deformation, $\Delta h/\Delta\tilde{h}$, on reduced nanoparticle size, $R_p/\tilde{R}_p$, for nanoparticles with different cross-linking densities, different strengths of the substrate–polymer interactions, and different nanoparticle sizes. For our new data set, the notations are the same as in Figure 4a and b. Simulations data from refs 39 and 44 are shown as brown pentagons. Solid line corresponds to eq 25 with values of the fitting parameters $A_G = 0.416$ and $B_G = 0.798$.

5. CONCLUSIONS

We have studied interactions of nanoparticles with patterned surfaces. Our simulations have shown that for elastic nanoparticles and gels the transition between Cassie–Baxter and Wenzel states is a first-order transition, which depends on the elastic properties of nanoparticles and gels, strength of interactions, and dimensions of the patterns. In the interval of parameter where both Cassie–Baxter and Wenzel states coexist, the equilibrium indentation depth produced by substrate posts in the contact region is a result of averaging between indentations produced in these two pure states. The scaling model of the contact free energy between patterned substrate and elastic nanoparticle qualitatively describes the first-order transition between Cassie–Baxter and Wenzel states with increasing nanoparticle shear modulus. Note that the transition between Cassie–Baxter and Wenzel states was also observed for liquid wetting of patterned surfaces as a function of substrate hydrophobicity and pattern dimensions.[23−26] In this respect, nanoparticle elastic properties play a role similar to droplet–substrate interactions and control nanoparticle–substrate affinity.

Analysis of the simulation data demonstrates that we can use an effective work of adhesion, W_{eff}, between nanoparticle and patterned substrate to describe nanoparticle shape deformation. This approach allowed us to map the problem of the nanoparticle interaction with patterned substrate to one describing interactions of nanoparticles and substrates of arbitrary rigidity.[39,44] In the framework of this approach, we have confirmed that there are two different regimes of nanoparticle substrate interactions. For small nanoparticles such that $R_p < \gamma_p^{3/2} G_p^{-1} W_{eff}^{-1/2}$, the equilibrium shape deformation of nanoparticle is a result of balance between capillary forces (wetting regime in Figure 11). However, for large nanoparticles $R_p > \gamma_p^{3/2} G_p^{-1} W_{eff}^{-1/2}$, the nanoparticle deformation is determined by balancing elastic energy of nanoparticle deformation with work of adhesion between nanoparticle and substrate (adhesion regime in Figure 11).

The presented here approach could be extended to describe interactions of nanoparticles with substrates covered with stripes and cylindrical post as well as substrates with fractal roughness. We hope to address these problems in the future.

DOI: 10.1021/la5045442
Langmuir XXXX, XXX, XXX−XXX

AUTHOR INFORMATION

Corresponding Author

*E-mail: avd@ims.uconn.edu.

Notes

The authors declare no competing financial interest.

ACKNOWLEDGMENTS

We are grateful to the National Science Foundation for financial support under Grant DMR-1409710. This work was performed at the U.S. Department of Energy, Center for Integrated Nanotechnologies, at Los Alamos National Laboratory (contract no. DE-AC52-06NA25396) and Sandia National Laboratories. Sandia is a multiprogram laboratory operated by Sandia Corporation, a Lockheed Martin Company, for the United States Department of Energy under contract no. DE-AC04-94AL85000. J.-M.Y.C's contribution was sponsored by the Office of Advanced Scientific Computing Research, U.S. Department of Energy, and performed at Oak Ridge National Laboratory, which is managed by UT-Battelle, LLC under contract no. De-AC05-00OR22725.

REFERENCES

(1) De Gennes, P.-G.; Brochard-Wyart, F.; Quéré, D. *Capillarity and Wetting Phenomena: Drops, Bubbles, Pearls, Waves*; Springer: New York, 2004.

(2) Liu, M.; Wang, S.; Jiang, L. Bioinspared multiscale surfaces with special wettability. *MRS Bull.* **2013**, *38*, 375−381.

(3) Bhushan, B.; Jung, Y. C. Wetting, adhesion and friction of superhydrophobic and hydrophilic leaves and fabricated micro/nanopatterned surfaces. *J. Phys.: Condens. Matter* **2008**, *20*, 225010-1−24.

(4) Blossey, R. Self-cleaning surfaces-Virtual realities. *Nat. Mater.* **2003**, *2*, 301−306.

(5) Barthlott, W.; Neinhuis, C. Purity of the sacred lotus, or escape from contamination in biological surfaces. *Planta* **1997**, *202*, 1−8.

(6) Gao, H. J.; Wang, X.; Yao, H. M.; Gorb, S.; Arzt, E. Mechanics of hierarchical adhesion structures of geckos. *Mech. Mater.* **2005**, *37*, 275−285.

(7) Gao, X. F.; Yan, X.; Yao, X.; Xu, L.; Zhang, K.; Zhang, J. H.; Yang, B.; Jiang, L. The dry-style antifogging properties of mosquito compound eyes and artificial analogues prepared by soft lithography. *Adv. Mater.* **2007**, *19*, 2213−2217.

(8) Huber, G.; Mantz, H.; Spolenak, R.; Mecke, K.; Jacobs, K.; Gorb, S.; Arzt, E. Evidence for capillarity contributions to gecko adhesion from single spatula nanomechanical measurements. *Proc. Natl. Acad. Sci. U.S.A.* **2005**, *102*, 16293−16296.

(9) Zheng, Y. M.; Bai, H.; Huang, Z. B.; Tian, X. L.; Nie, F. Q.; Zhao, Y.; Zhai, J.; Jiang, L. Directional water collection on wetted spider silk. *Nature* **2010**, *463*, 640−643.

(10) Ju, J.; Bai, H.; Zheng, Y. M.; Zhao, T.; Fang, R.; Jiang, L. A multi-structural and multi-functional integrated fog collection system in cactus. *Nat. Commun.* **2012**, *3*, 1247.

(11) Quéré, D. Wetting and roughness. *Annu. Rev. Mater. Res.* **2008**, *38*, 71−99.

(12) Wenzel, R. N. Resistance of solid surfaces to wetting by water. *Ind. Eng. Chem.* **1936**, *28*, 988−994.

(13) Cassie, A. B. D.; Baxter, S. Wettability of porous surfaces. *Trans. Faraday Soc.* **1944**, *40*, 546−551.

(14) Cassie, A. B. D. Contact angles. *Discuss. Faraday Soc.* **1948**, *3*, 11−16.

(15) Bico, J.; Thiele, U.; Quéré, D. Wetting of textured surfaces. *Colloids Surf., A* **2002**, *206*, 41−46.

(16) Bormashenko, E.; Pogreb, R.; Stein, T.; Whyman, G.; Erlich, M.; Musin, A.; Machavariani, V.; Aurbach, D. Characterization of rough surfaces with vibrated drops. *Phys. Chem. Chem. Phys.* **2008**, *10*, 4056−4061.

(17) Lafuma, A.; Quéré, D. Superhydrophobic states. *Nat. Mater.* **2003**, *2*, 457−460.

(18) Sabragaglia, M.; Peters, A. M.; Pirat, C.; Borkent, B. M.; Lammertink, R. G. H.; Wessling, M.; Lohse, D. Spontaneous breakdown of superhydrophobicity. *Phys. Rev. Lett.* **2007**, *99*, 156001-1−4.

(19) Kwon, H.-M.; Paxson, A. T.; Varanasi, K. K.; Patankar, N. A. Rapid deceleration-driven wetting transition during pandant drop deposition on superhydrophobic surfaces. *Phys. Rev. Lett.* **2011**, *106*, 036102-1−4.

(20) Papadopoulos, P.; Mammen, L.; Deng, X.; Vollmer, D.; Butt, H.-J. How superhydrophobicity breaks down. *Proc. Natl. Acad. Sci. U.S.A.* **2013**, *110*, 3254−3258.

(21) Checco, A.; Ocko, B. M.; Rahman, A.; Black, C. T.; Tasinkevych, M.; Giacomello, A.; Dietrich, S. Collapse and reversibility of the superhydrophobic state on nanotextured surfaces. *Phys. Rev. Lett.* **2014**, *112*, 216101-1−4.

(22) Murakami, D.; Jinnai, H.; Takahara, A. Wetting transition from the Cassie-Baxter state to Wenzel state on textured polymer surfaces. *Langmuir* **2014**, *30*, 2061−2067.

(23) Bormashenko, E. Progress in understanding wetting transition on rough surfaces. *Adv. Colloid Interface Sci.* **2014**, DOI: 10.1016/j.cis.2014.02.009.

(24) Koishi, T.; Yasuoka, K.; Fujikawa, S.; Ebisuzaki, T.; Zheng, X. C. Coexistence and transition between Cassie and Wenzel state on pillared hydrophobic surface. *Proc. Natl. Acad. Sci. U.S.A.* **2009**, *106*, 8435−8440.

(25) Khan, S.; Singh, J. K. Wetting transition of nanodroplets of water on textured surfaces:a molecular dynamics study. *Mol. Simul.* **2014**, *40*, 458−468.

(26) Savoy, E. S.; Escobedo, F. A. Simulation study of free-energy barriers in the wetting transition of an oily fluid on a rough surface with reentrant geometry. *Langmuir* **2012**, *28*, 16080−16090.

(27) Giacomello, A.; Chinappi, M.; Meloni, S.; Casciola, C. M. Metastable wetting on superhydrophobic surfaces: Continuum and atomistic views of the Cassie-Baxter-Wenzel transition. *Phys. Rev. Lett.* **2012**, *109*, 226102-1−4.

(28) Shahraz, A.; Borhan, A.; Fichthorn, K. A. Wetting on physically paterned solid surfaces: the relevance of molecular dynamics simulations to macroscopic systems. *Langmuir* **2013**, *29*, 11632−11639.

(29) Yong, X.; Zhang, L. T. Nanoscale wetting on groove-patterned surfaces. *Langmuir* **2009**, *25*, 5045−5053.

(30) Grzelak, E. M.; Errington, J. R. Nanoscale limit to the applicability of wenzel's equation. *Langmuir* **2010**, *26*, 13297−13304.

(31) Fuller, K. N. G.; Tabor, D. The effect of surface roughness on the adhesion of elastic solids. *Proc. R. Soc. A* **1975**, *345*, 327−342.

(32) Persson, B. N. J.; Tosatti, E. The effect of surface roughness on the adhesion of elastic solids. *J. Chem. Phys.* **2001**, *115*, 5597−5610.

(33) Persson, B. N. J. Adhesion between an elastic body and a randomly rough hard surface. *Eur. Phys. J. E* **2002**, *8*, 385−401.

(34) Persson, B. N. J. Contact mechanics for layered materials with randomly rough surfaces. *J. Phys.: Condens. Matter* **2012**, *24*, 095008.

(35) Persson, B. N. J.; Gorb, S. The effect of surface roughness on the adhesion of elastic plates with application to biological systems. *J. Chem. Phys.* **2003**, *119*, 11437−11444.

(36) Pastewka, L.; Robbins, M. O. Contact between rough surfaces and a criterion for macroscopic adhesion. *Proc. Natl. Acad. Sci. U.S.A.* **2014**, *111*, 3298−3303.

(37) Johnson, K. L. *Contact Mechanics*, 9th ed.; Cambridge University Press: UK, 2003.

(38) Carrillo, J.-M. Y.; Dobrynin, A. V. Molecular dynamics simulations of nanoimprinting lithography. *Langmuir* **2009**, *25*, 13244−13249.

(39) Carrillo, J.-M. Y.; Raphael, E.; Dobrynin, A. V. Adhesion of nanoparticles. *Langmuir* **2010**, *26*, 12973−12979.

(40) Carrillo, J.-M. Y.; Dobrynin, A. V. Contact mechanics of nanoparticles. *Langmuir* **2012**, *28*, 10881−10890.

DOI: 10.1021/la5045442
Langmuir XXXX, XXX, XXX−XXX

(41) Salez, T.; Benzaquen, M.; Raphaël, É. From adhesion to wetting of a soft particle. *Soft Matter* **2013**, *9*, 10699−10704.
(42) Style, R. W.; Hyland, C.; Boltyanskiy, R.; Wettlaufer, J. S.; Dufresne, E. R. Surface tension and contact with soft elastic solids. *Nat. Commun.* **2013**, *4*, 2728.
(43) Xu, X.; Jagota, A.; Hui, C.-Y. Effect of Surface Tension on the Adhesive Contact of a Rigid Sphere to a Compliant Substrate. *Soft Matter* **2014**, *10*, 4625−4632.
(44) Cao, Z.; Stevens, M. J.; Dobrynin, A. V. Adhesion and wetting of nanoparticles on soft surfaces. *Macromolecules* **2014**, *47*, 3203−3209.
(45) Frenkel, D.; Smit, B. *Understanding Molecular Simulation: From Algorithms to Applications*; Academic Press: New York, 2001.
(46) Kremer, K.; Grest, G. S. Dynamics of entangled linear polymer melts: A molecular - dynamics simulation. *J. Chem. Phys.* **1990**, *92*, 5057−5086.
(47) Plimpton, S. Fast parallel algorithms for short-range molecular dynamics. *J. Comput. Phys.* **1995**, *117*, 1−19.
(48) Kumar, S.; Rosenberg, J. M.; Bouzida, D.; Swendsen, R. H.; Kollman, P. A. Multidimensional free-energy calculations using the Weighted Histogram Analysis Method. *J. Comput. Chem.* **1995**, *16*, 1339.

DOI: 10.1021/la5045442
Langmuir XXXX, XXX, XXX−XXX